



Diffraction Tomography Using Born Approximation

S. Banerjee⁽¹⁾

Indian Institute of Technology, Delhi

Kolkata India

soumyadip.banerjee@gmail.com

Abstract— This paper mainly describes a new method to solve forward and backward problem related to 2D diffraction tomography. The method is based upon Born approximation which holds for weakly scattering body. A new approach to mapping is presented from real space to K-space. The reconstructed images are obtained for different SNR values and also for different resolution in K space. Also suitable forward and inverse formulas are presented for the following method.

Index Terms— Diffraction tomography, K-space, Ewald's circle, Fourier transform, Born approximation

I. INTRODUCTION

The last two decades has seen an immense growth in the development of new algorithms and techniques in diffraction tomography problems. Though non-diffracting tomography is more popular in medical applications, still when it comes to reconstruction of the shape and the electrical properties (complex refractive index profile) of the body under test, diffraction tomography has an advantage. Early techniques employed Fourier diffraction theorem [6] to obtain data in frequency domain and that data is processed using an inverse algorithm [2] to get back the reconstructed image. Unlike the direct methods which work on far field data, there are methods which work on near field

data and the reconstruction occurs through an iterative process and is based on moment method solution [10].

This paper is organised as follows. First the theoretical background is provided for both 2D diffraction tomography. Under 2D tomography the mathematical foundation for the two new scanning methods are explained and corresponding to the methods the forward and the inverse formulas are provided. A suitable forward and reconstruction formula is also provided. Secondly, there is the Simulation and Result section where the above methods are tested on different test bodies and the reconstructed images are shown for different cases. Finally, conclusion of the work is provided.

II. THEORY

Considering an inhomogeneous medium for which the Helmholtz equation is given by

$$[\nabla^2 + k^2]\mathbf{u}(\mathbf{r}) = 0 \quad (1)$$

Where, $k(\mathbf{r}) = k_0 n(\mathbf{r})$

k_0 = average wave no. of the medium.

$n(\mathbf{r})$ is complex refractive index of the medium given by

$$n(\mathbf{r}) = \sqrt{\frac{\mu(\mathbf{r}) \epsilon(\mathbf{r})}{\mu_0 \epsilon_0}}$$

$u(\mathbf{r})$ =Complex amplitude of the total field at position given by \mathbf{r} .

The above equation can be rewritten as

$$[\nabla^2 + k_0^2] \mathbf{u}_s(\mathbf{r}) = -\mathbf{u}(\mathbf{r})F(\mathbf{r}) \quad (2)$$

Where, $F(\mathbf{r}) = k_0^2[n^2(\mathbf{r})-1]$

$F(\mathbf{r})$ is the forcing function called the scattering potential and $\mathbf{u}_s(\mathbf{r})$ is the complex amplitude of the scattered field.

The solution to (2) obtained by green's function method is given as

$$\mathbf{u}_s(\mathbf{r}) = \int F(\mathbf{r}', \omega) g(\mathbf{r} | \mathbf{r}') u(\mathbf{r}') dv \quad (3)$$

Where, $g(\mathbf{r}|\mathbf{r}')$ is the green's function used in the solution.

The above solution (3) is a Fredholm equation of second kind. Though there are standard theoretical and numerical methods [5] to solve the equation. But if the test body has weak inhomogeneity then the above equation can be simplified using first order Born approximation [6]. In this approximation the total field in (3) is replaced by the incident field $u_0(\mathbf{r})$ and hence the simplified equation is given by

$$\mathbf{u}_s(\mathbf{r}) = \int F(\mathbf{r}', \omega) g(\mathbf{r} | \mathbf{r}') u_0(\mathbf{r}') dv \quad (4)$$

where, in 2D case the Green's function is given by

$$g(\mathbf{r} | \mathbf{r}') = -\frac{j}{4} H_0^2(k_0|\mathbf{r} - \mathbf{r}'|)$$

A. Forward Problem

In 2D diffraction tomography the test object or objects are considered to be having refractive index variation along the cross-section and having no or gradual variation with height. Under far field approximation [6] the scattered field at the observation point is given by

$$\mathbf{u}_s(\mathbf{r}) = A_0 \sqrt{\frac{2j}{\pi k_0 r}} e^{-jk_0 r} f(\mathbf{s}_0, \mathbf{s}) \quad (5)$$

Where, A_0 = amplitude of the incident field

\mathbf{s}_0 =unit vector along the direction of propagation of the incident field.

\mathbf{s} = unit vector directed towards the position of the receiver Rx

$f(\mathbf{s}_0, \mathbf{s})$ is called the Scattering amplitude and is given as

$$f(\mathbf{s}_0, \mathbf{s}) = F'[\mathbf{K}] = \iint F(\mathbf{r}', \omega) e^{-j\mathbf{K} \cdot \mathbf{r}'} ds \quad (6)$$

Here, $\mathbf{K} = k_0(\mathbf{s}-\mathbf{s}_0)$ is called the spatial frequency vector[6]. The significance of (6) is that the complex amplitude of the scattered field measured in the far field region depends entirely on only one Fourier component of the scattering potential $F(\mathbf{r})$ corresponding to a given \mathbf{K} vector. The approach in this type of problem is to obtain Fourier component data for all \mathbf{K} vectors within the \mathbf{K} space. For that the scattered field is to be measured at all possible direction \mathbf{s} and also for all possible direction of the incident wave \mathbf{s}_0 . This is best diagrammatically described by Ewald's circle of reflection. For a fixed \mathbf{k}_0 and different orientation of \mathbf{k} the \mathbf{K} vector traces out this Ewald's circle of reflection. In 3D case the circle transforms into a sphere. The \mathbf{K} space is bounded by the outer circle of radius given by $K=2k_0$

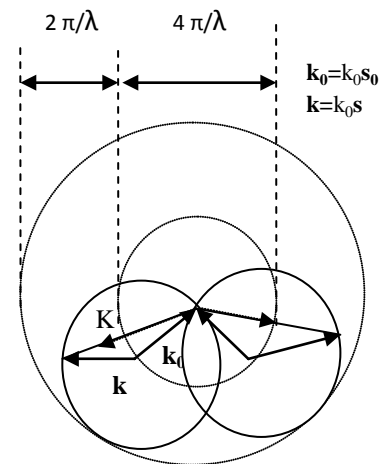


Fig. 1. The figure showing the construction of a \mathbf{K} vector from \mathbf{k} and \mathbf{k}_0 vector and the Ewald's circle it traces out for two possible orientation of \mathbf{k}_0 vector.

Two methods are suggested to solve the forward problem. It is seen from (6) that the 2D Fourier transform value f depends mainly on \mathbf{K} . Generally, Fourier diffraction theorem is applied to obtain f data for different position of receiver and also for different angle of incidence. But this leads to a non-linear mapping from real space to \mathbf{K} space. This makes the reconstruction procedure difficult. To circumvent the situation the sampled values of the scattered field is extracted at non-uniform intervals in real space so that the f data are obtained for uniform sampled values of \mathbf{K} . This makes the reconstruction problem easier to handle.

In the first method (Method I) the K space is pictured with the help of a Cartesian co-ordinate system, where it is divided into uniform cells of size ΔK as shown in the figure below

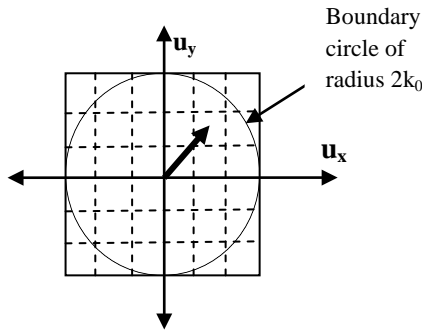


Fig. 2. Representation of K space in Cartesian co-ordinate system. The dark arrow representing to a K vector pointing to one of the cell.

In order to obtain f data corresponding to each cell the transmitting and the receiving antenna should be properly oriented with respect to the test body in the far field region. An effective way of doing this is to make the transmitter fixed and change the angular position of the receiver accompanied by a proper rotation of the body to a particular angle.

Let $\mathbf{K} = K_x \mathbf{u}_x + K_y \mathbf{u}_y = m\Delta K \mathbf{u}_x + n\Delta K \mathbf{u}_y$
and $\Delta K = 2k_0/M$,

where m and n are rational no.s and $(2M)^2$ is the total no. of cells the K space is divided into.

The Tx antenna position on a unit radius circle is fixed and is given by

$$X_{Tx} = 1 \quad Y_{Tx} = 0$$

The Rx antenna position on a unit radius circle is given by

$$X_{Rx} = -\cos(\alpha - \alpha_0) \quad Y_{Rx} = \sin(\alpha - \alpha_0)$$

$$\text{Where, } \alpha_0 = \tan^{-1} \frac{n}{m} + \cos^{-1} \frac{\sqrt{(m^2 + n^2)}}{M} \quad (7)$$

$$\text{and, } \alpha = \tan^{-1} \left[\frac{\sin \alpha_0 - 2 \frac{n}{M}}{\cos \alpha_0 - 2 \frac{m}{M}} \right] \quad (8)$$

In order to obtain proper incident field direction the test body is rotated by an angle $\pi - \alpha_0$ in anti-clockwise direction.

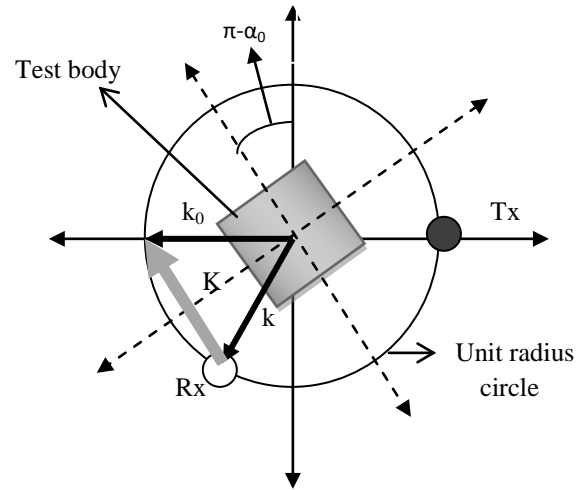


Fig. 3. Diagram showing the arrangement of Tx, Rx and the body for the Method I type scanning.

The forward formula for obtaining the scattering amplitude value is obtained by dividing the entire body or the scattering region into N no. of square cells of side length h. For a given K vector f is given by

$$f(\mathbf{K}) = h^2 \text{sinc}\left(\frac{K_x h}{2}\right) \text{sinc}\left(\frac{K_y h}{2}\right) \sum_{i=1}^N F(r_i') e^{-j \mathbf{K} \cdot \mathbf{r}_i'} \quad (9)$$

Where, $\mathbf{r}_i' = x_i' \mathbf{u}_x + y_i' \mathbf{u}_y$ is the position vector of the i^{th} cell of the scattering region and h^2 is the cell area.

2.3 Backward Problem

As the K-space is divided into uniform cells, so the low pass filtered approximation of the scattering potential [6] can be written as

$$F_{LP}(\mathbf{r}) = \left(\frac{\Delta K}{2\pi}\right)^2 \text{sinc}\left(\frac{\Delta K x}{2}\right) \text{sinc}\left(\frac{\Delta K y}{2}\right) \sum_{i=1}^{(2M)^2} f(K_i) e^{j K_i \cdot \mathbf{r}} \quad (10)$$

ΔK^2 = area of each cell in K-space.

Here, \mathbf{K}_i specifies the position vector of the i^{th} cell in K-space. The above discrete sum is to be evaluated within the boundary circle.

III. Numerical Model

The numerical model of two different test bodies is presented in this section. The first body considered is a 2D body with mainly three types of scatterers placed at different locations and having different refractive index

profile. While the second body considered is a high contrast body compared to the first comprising of bones and muscles. The shape of the bones are approximated to square in nature instead of being irregular. The body image of both the bodies are divided into 2500(50^2) cells.

A. *Body Model A*

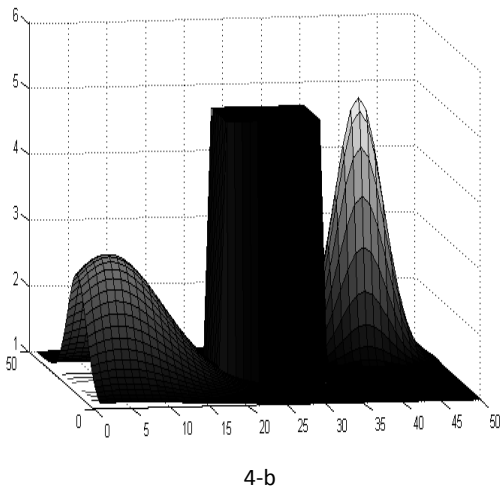
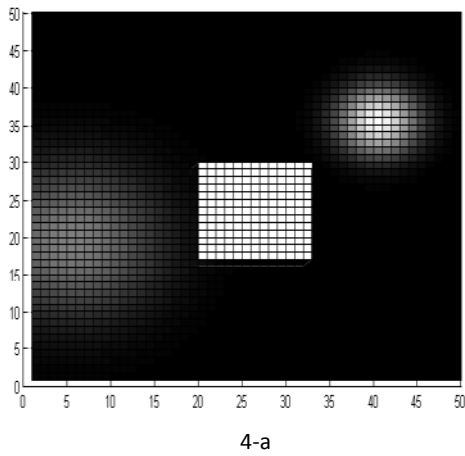
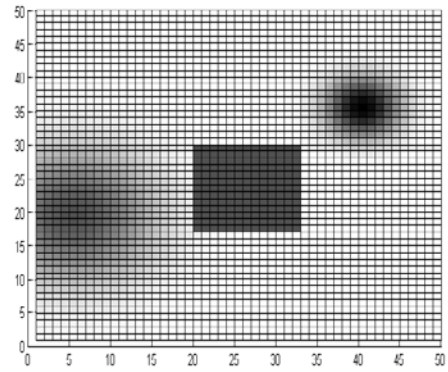
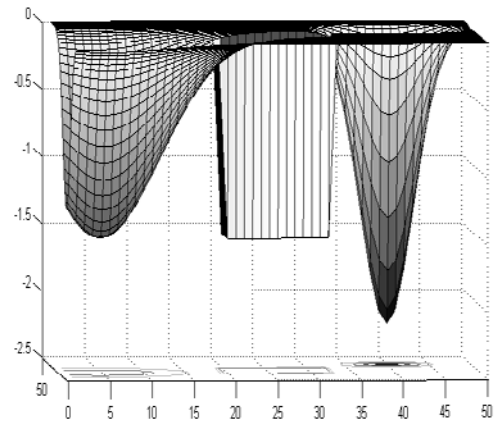


Fig-4(a) figure showing the position and the shape of the scatterers in the region R' (extent of R' is 10cmX10cm) of Body A (b) figure depicting the real part of the refractive (n_r) index of the object(at 10GHz)



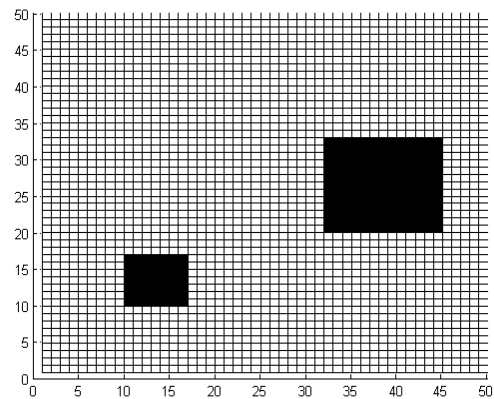
5-a



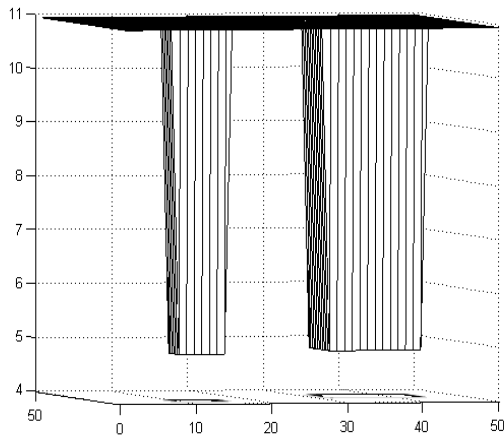
5-b

Fig-5(a) figure showing the position and the shape of the scatterers in the region R' (extent of R' is 10cmX10cm) (b) figure depicting the imaginary part of the refractive (n_i) index of the object (at 10GHz)

B. *Body Model B*

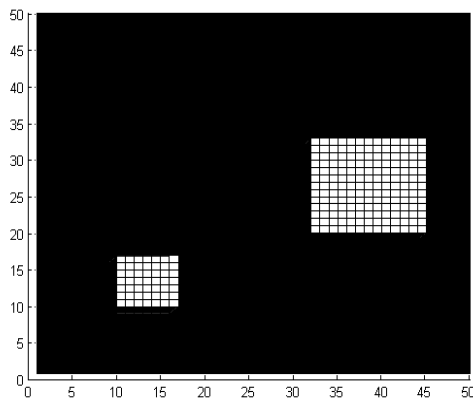


6-a

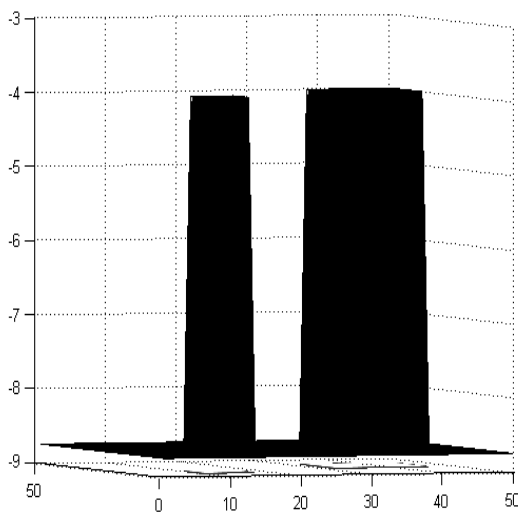


6-b

Fig-6(a) figure showing the position and the shape of the scatterers in the region R' (extent of R' is 10cmX10cm) of Body B(b) figure depicting the real part of the refractive (n_r) index of the object(at 10GHz)



7-a



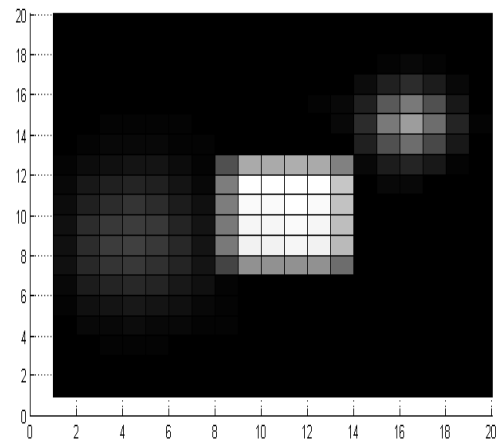
7-b

Fig-7(a) figure showing the position and the shape of the scatterers in the region R' (extent of R' is 10cmX10cm) of Body B(b) figure depicting the imaginary part of the refractive (n_i) index of the object(at 10GHz)

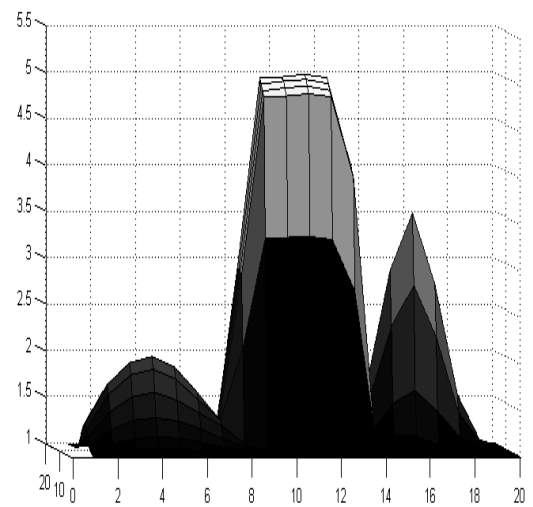
IV. Results and Discussion

The reconstructed images of the bodies are presented for two separate cases i.e. for method I and II. For each method the reconstructed images are obtained for high and low resolution in K-space. The inverse methods are tested with signals corrupted with different amount of noise. The type of noise considered over here is an Additive White Gaussian Noise (AWGN). The frequency of operation is 10GHz and the incident field amplitude is 1V/m for each case.

The results of the body model A is shown in fig 8,9 and 10 under different noise condition and considering high resolution in K space.. The no. of cells in K space is considered to be $2500(50)^2$. The no. of cells of the reconstructed image is $400(20)^2$.



8-a



8-b

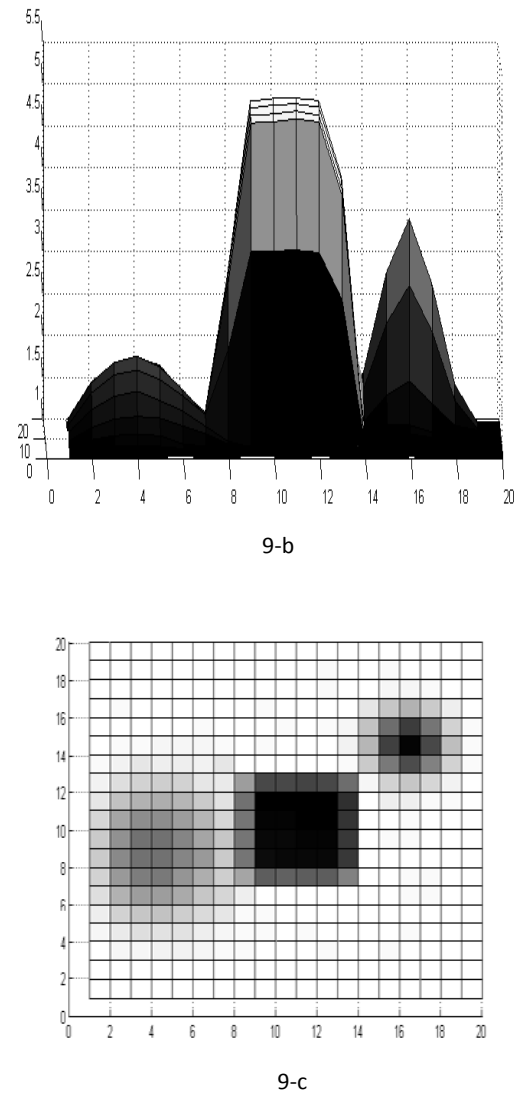
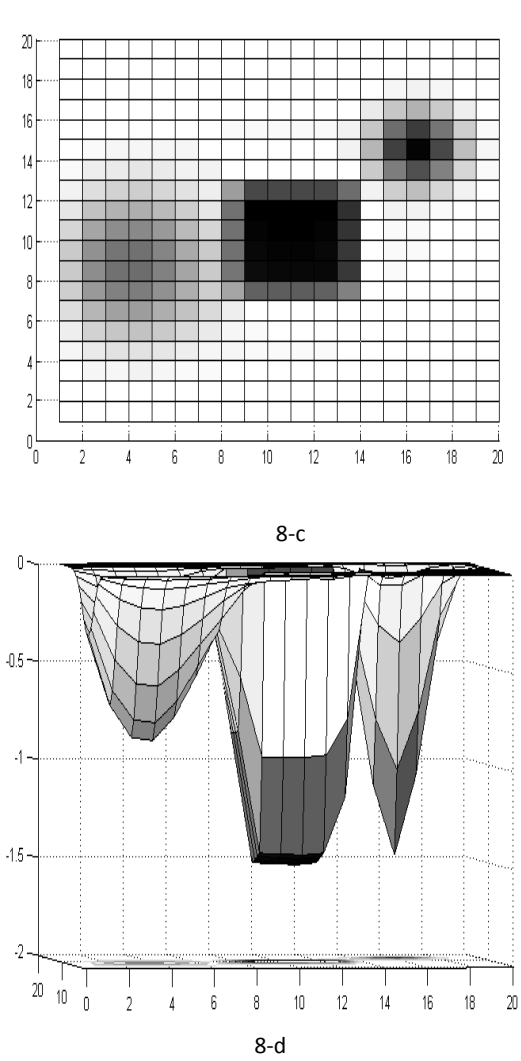


Fig-8 Reconstructed images of body A for high resolution in K-space. The profile of the real part of the refractive index obtained is shown in a and b while the imaginary part shown in c and d. The images are obtained under noise free condition.

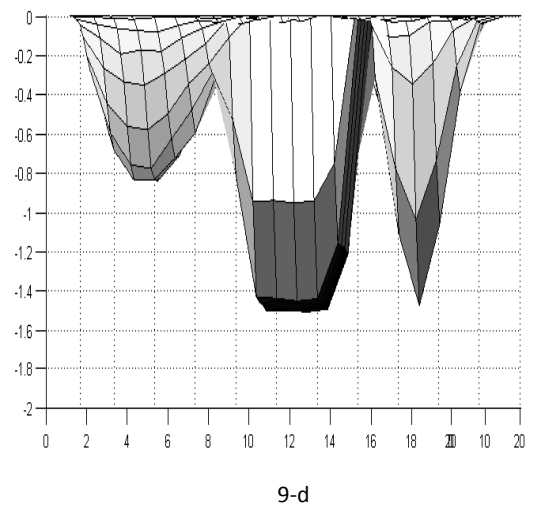
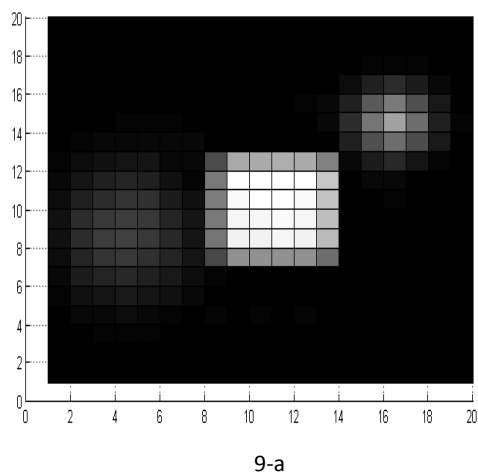
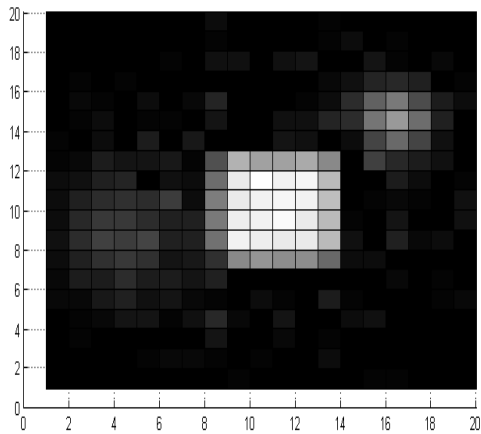
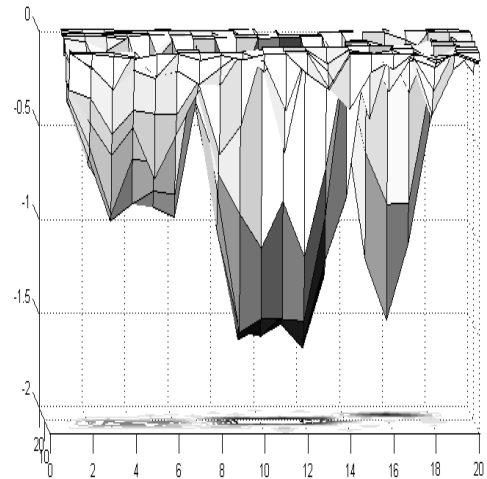


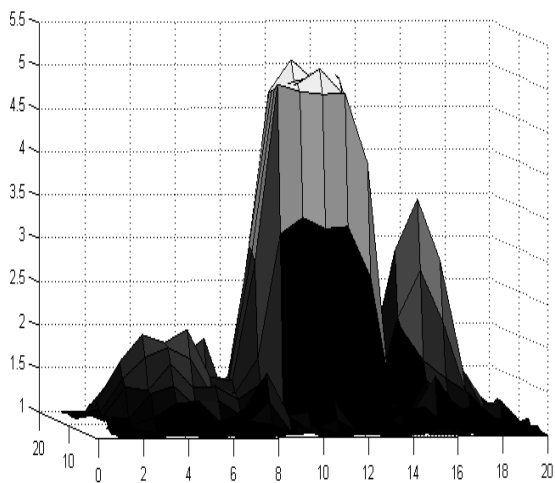
Fig-9 Reconstructed images of body A for high resolution in K-space. The profile of the real part of the refractive index obtained is shown in a and b while the imaginary part shown in c and d. The images are obtained under SNR=30dB



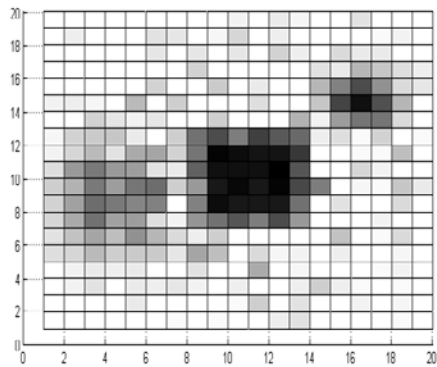
10-a



10-d



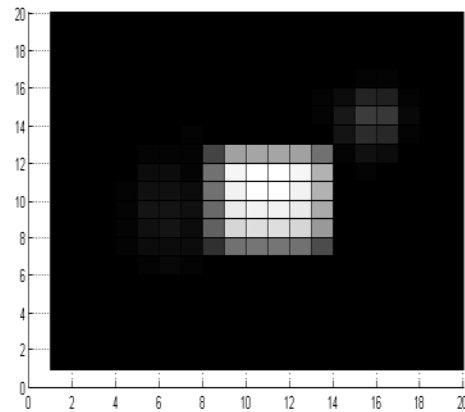
10-b



10-c

Fig-10 Reconstructed images of body A for high resolution in K-space. The profile of the real part of the refractive index obtained is shown in a and b while the imaginary part shown in c and d. The images are obtained under SNR=10dB

The results of the body model A is shown in fig 11-13 under different noise condition and considering low resolution in K space.. The no. of cells in K space is considered to be $900(30)^2$. The no. of cells of the reconstructed image is $400(20)^2$.



11-a

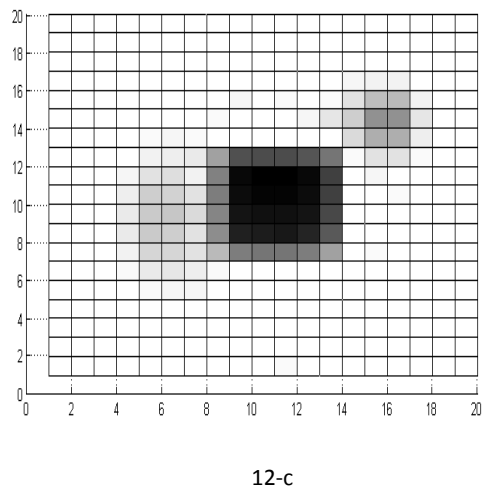
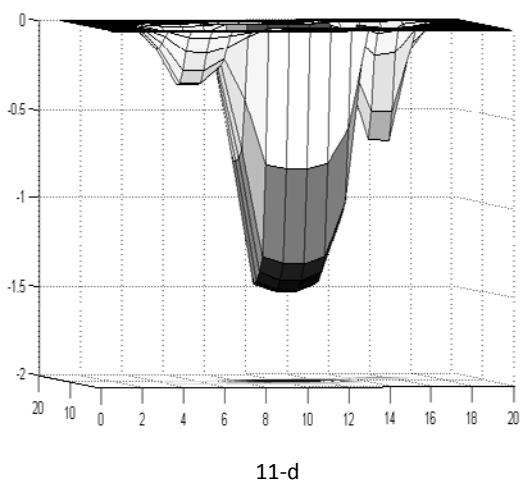
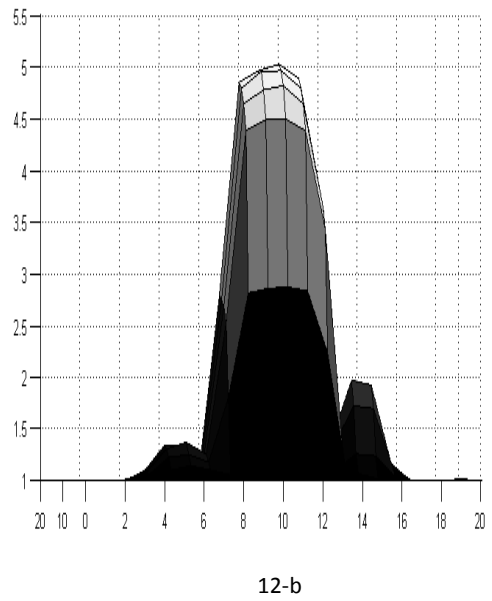
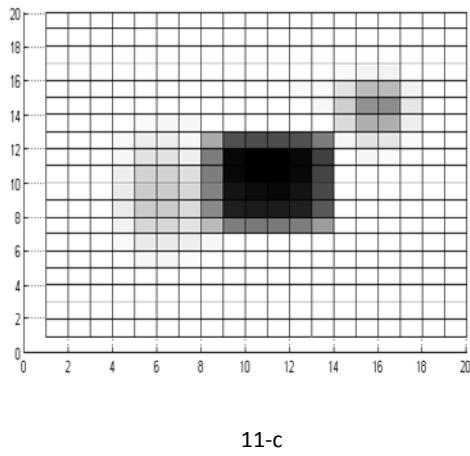
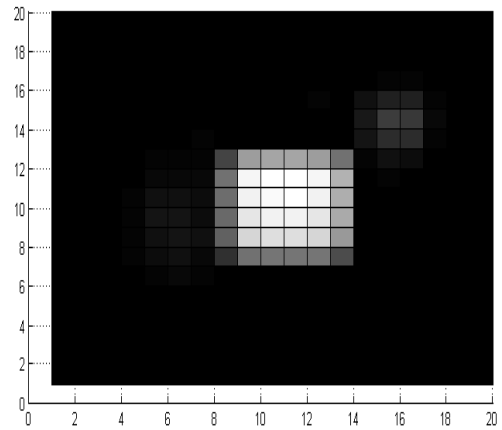
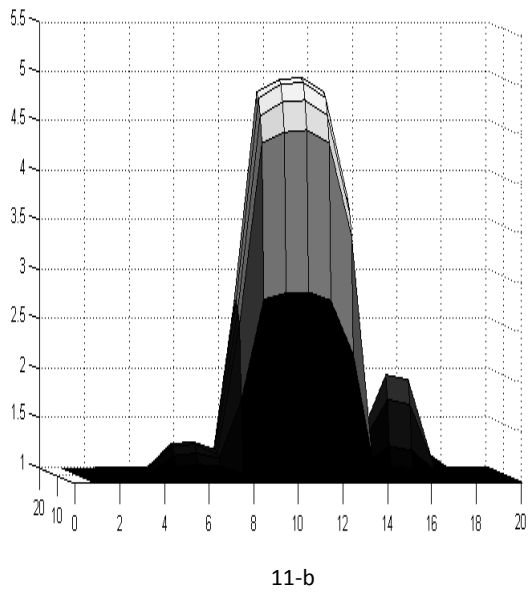
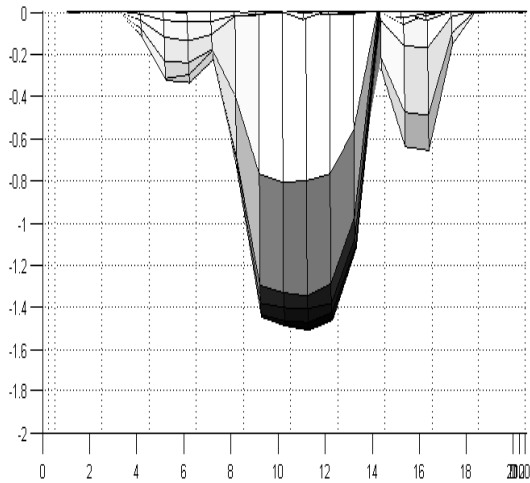
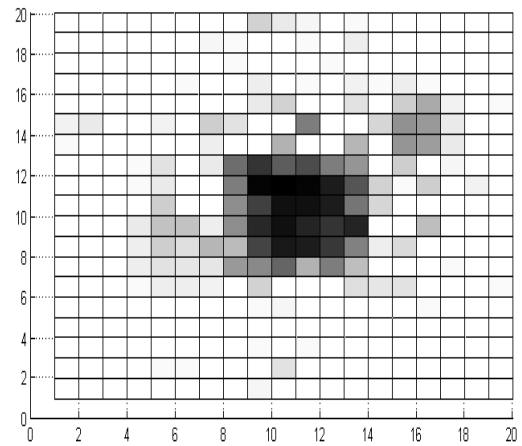


Fig-11 Reconstructed images of body A for low resolution in K-space. The profile of the real part of the refractive index obtained is shown in a and b while the imaginary part shown in c and d. The images are obtained under noise free condition.

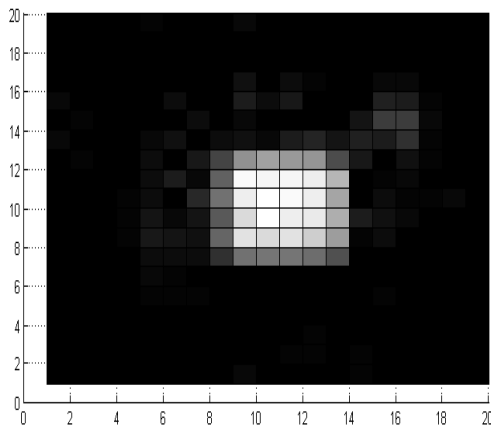


12-d

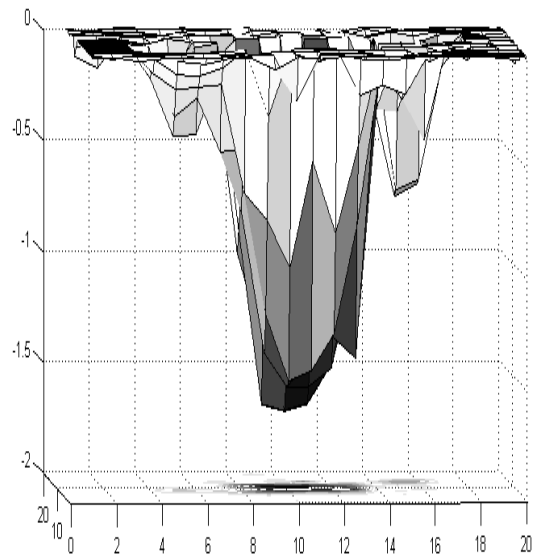


13-c

Fig-12 Reconstructed images of body A for low resolution in K-space. The profile of the real part of the refractive index obtained is shown in a and b while the imaginary part shown in c and d. The images are obtained under SNR-30 dB.

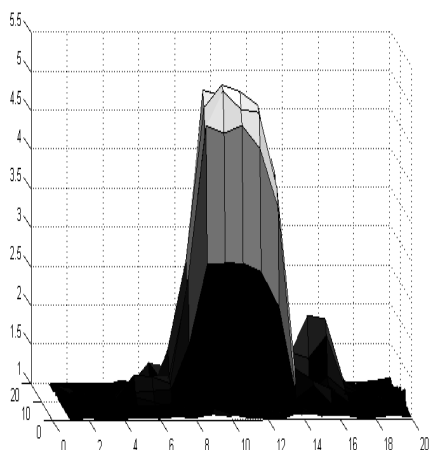


13-a



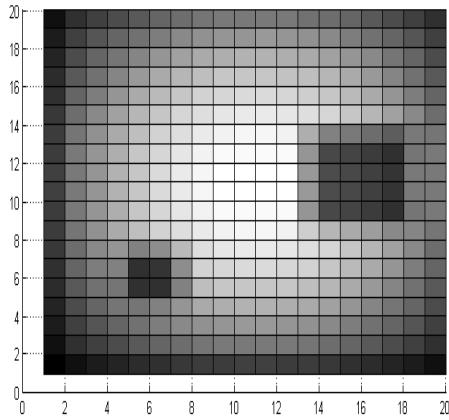
13-d

Fig-13 Reconstructed images of body A for low resolution in K-space. The profile of the real part of the refractive index obtained is shown in a and b while the imaginary part shown in c and d. The images are obtained under SNR-10 dB.

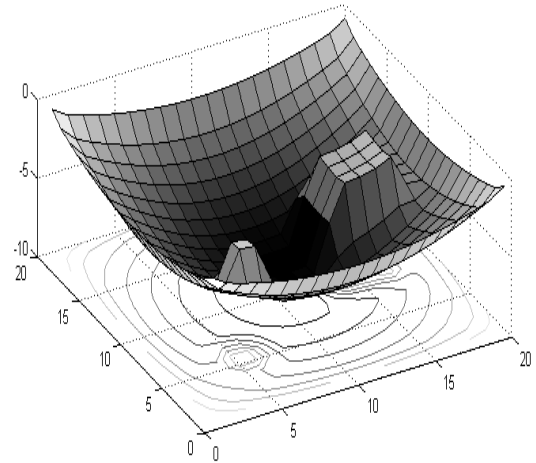


13-b

The results of the body model B is shown in fig 14,15 and 16 under different noise condition and considering high resolution in K space.. The no. of cells in K space is considered to be $2500(50)^2$. The no. of cells of the reconstructed image is $400(20)^2$.

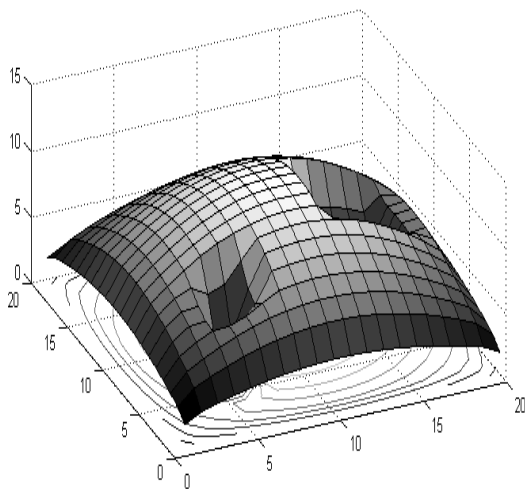


14-a

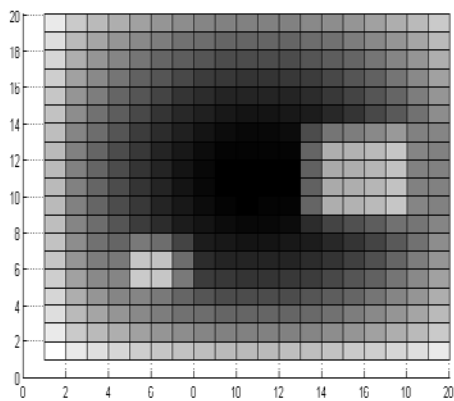


14-d

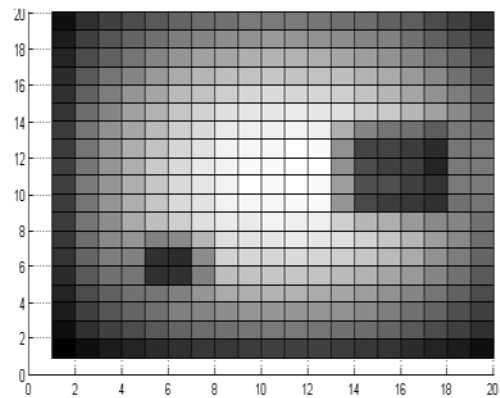
Fig-14 Reconstructed images of body A for high resolution in K-space. The profile of the real part of the refractive index obtained is shown in a and b while the imaginary part shown in c and d. The images are obtained under noise free condition.



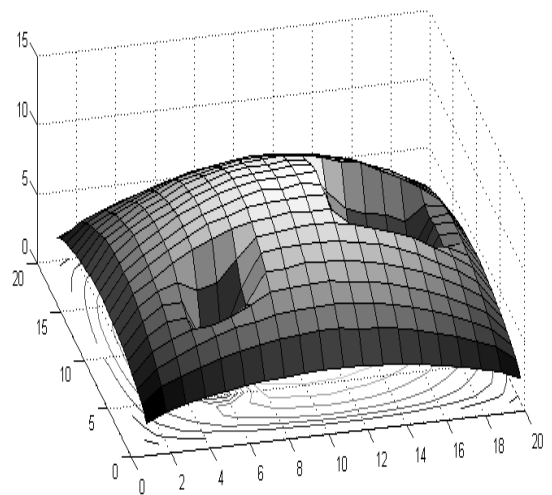
14-b



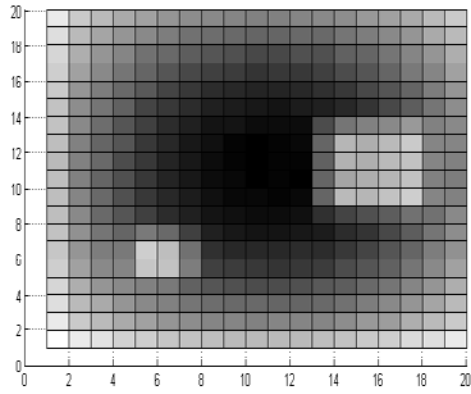
14-c



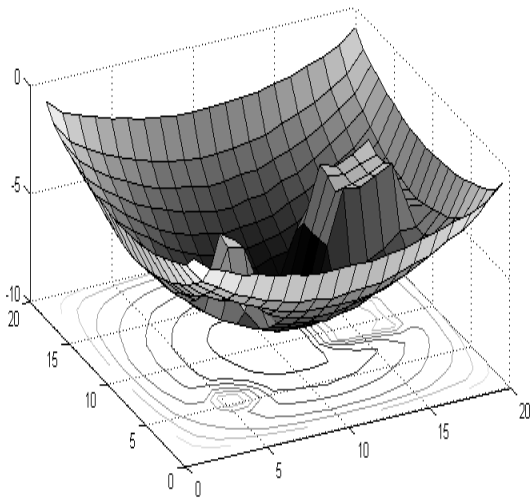
15-a



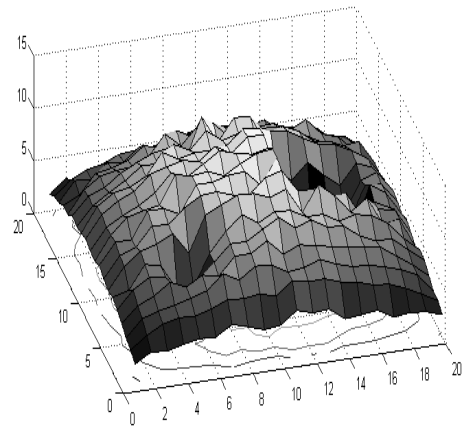
15-b



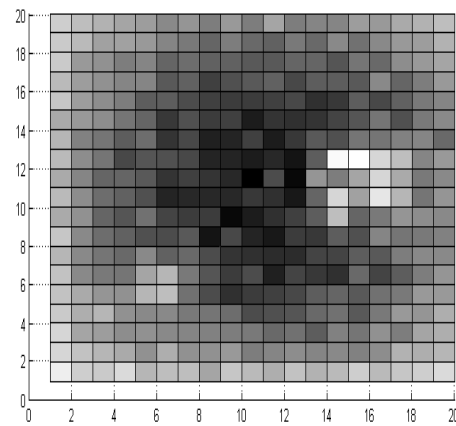
15-c



15-d

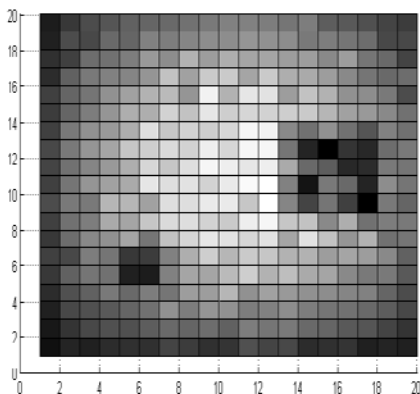


16-b

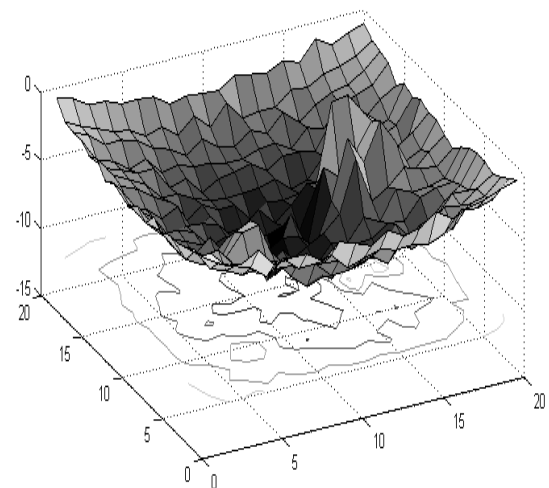


16-c

Fig-15 Reconstructed images of body A for high resolution in K-space. The profile of the real part of the refractive index obtained is shown in a and b while the imaginary part shown in c and d. The images are obtained under SNR-30 dB.



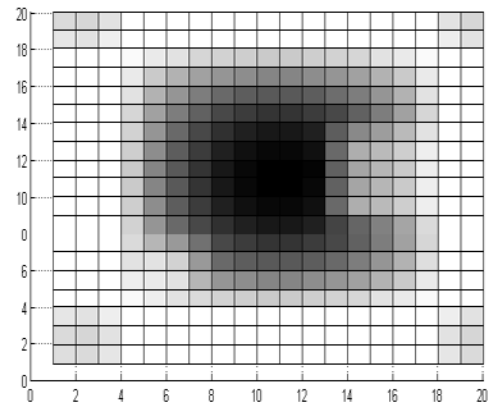
16-a



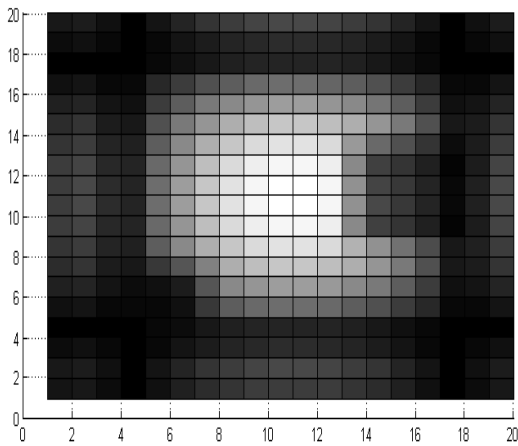
16-d

Fig-16 Reconstructed images of body A for high resolution in K-space. The profile of the real part of the refractive index obtained is shown in a and b while the imaginary part shown in c and d. The images are obtained under SNR-10 dB.

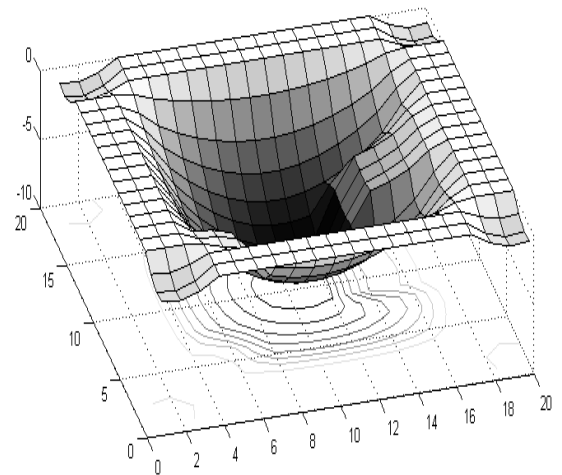
The results of the body model B is shown in fig 17-19 under different noise condition and considering high resolution in K space.. The no. of cells in K space is considered to be $900(30)^2$. The no. of cells of the reconstructed image is $400(20)^2$.



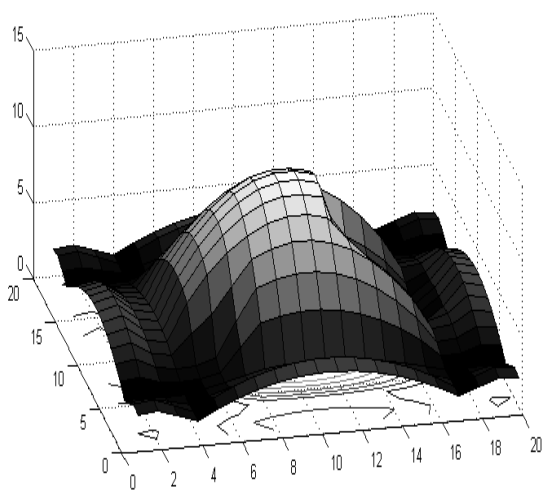
17-c



17-a

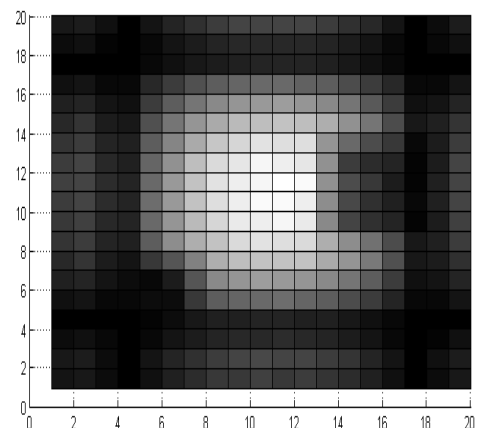


17-d

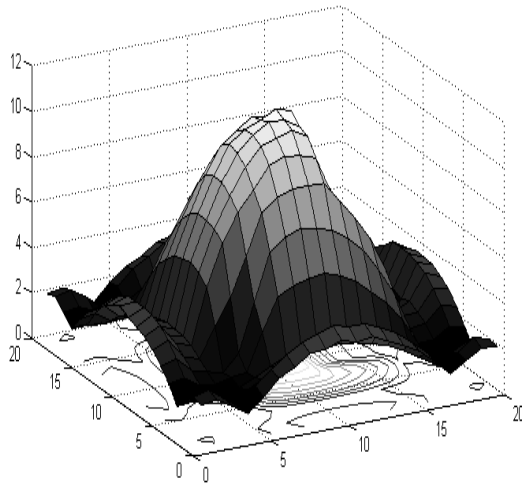


17-b

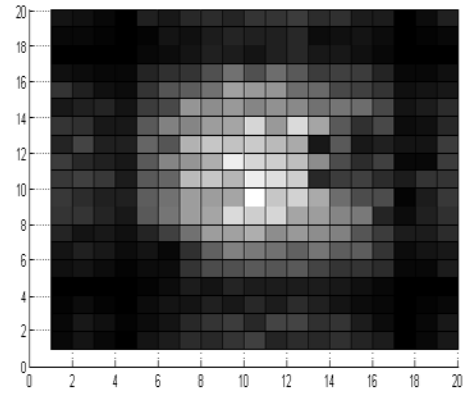
Fig-17 Reconstructed images of body A for low resolution in K-space. The profile of the real part of the refractive index obtained is shown in a and b while the imaginary part shown in c and d. The images are obtained under noise free condition.



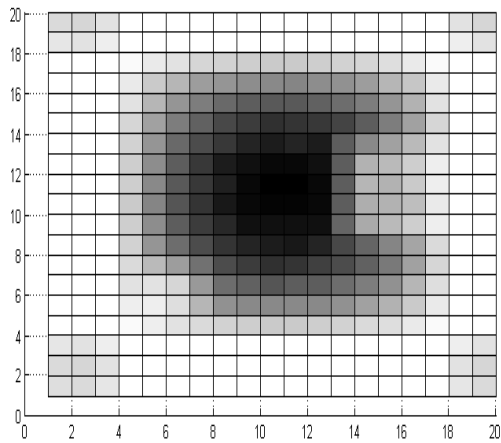
18-a



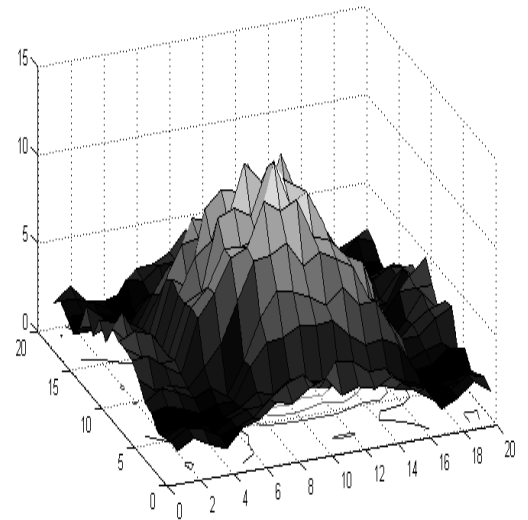
18-b



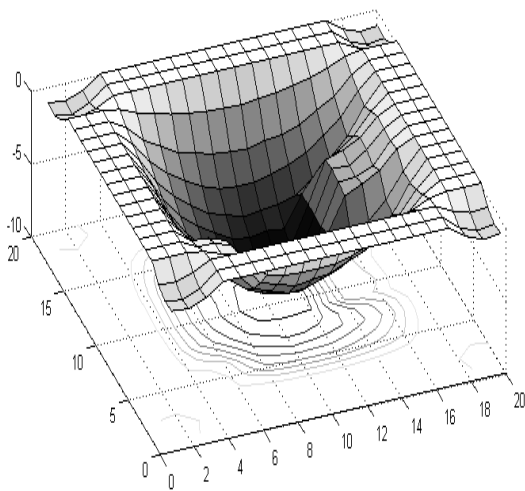
19-a



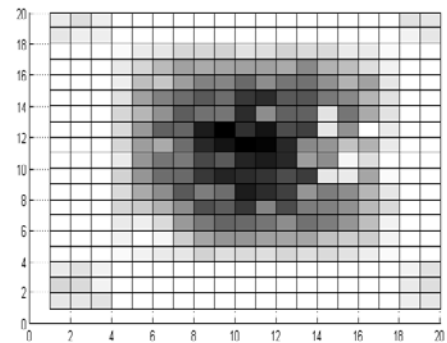
18-c



19-b



18-d



19-c

Fig-18 Reconstructed images of body A for low resolution in K-space. The profile of the real part of the refractive index obtained is shown in a and b while the imaginary part shown in c and d. The images are obtained under SNR-30 dB.

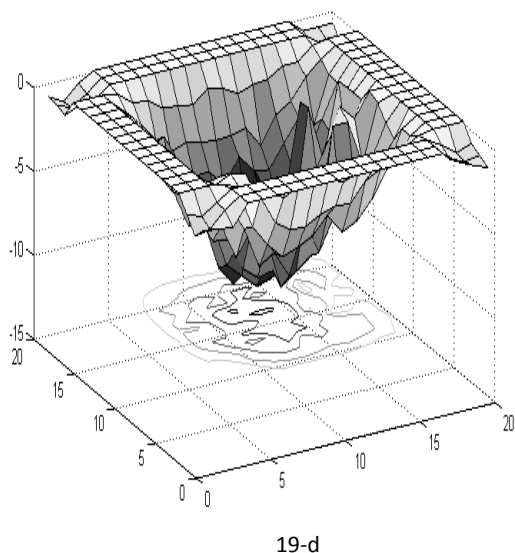


Fig-19 Reconstructed images of body A for low resolution in K-space. The profile of the real part of the refractive index obtained is shown in a and b while the imaginary part shown in c and d. The images are obtained under SNR-10 dB.

When the reconstructed images are compared under the same noise condition then it is observed that the quality of the image is better when high resolution in K space is considered. This is more visible for images associated with low SNR values where it is hard to recover the profile of the body. The reconstructed images obtained in case of body model 2 is more erroneous than in case of body model 1. This is due to the fact that the methods described are based on Born Approximation which treats the body to be weakly scattering whereas body 2 is a high contrast body and is highly scattering. The main practical challenge in these direct methods is to extract the phase information from the received signal. This requires sophisticated technologies like the use of vector analysers. Other challenge is the proper positioning of Tx and Rx in the far field region.

The future work will be to modify the above method so that reconstruction of high contrast bodies can be done with more precision.

REFERENCES

1. A.C. Kak and M. Slaney , “Principles of Computerised Tomographic Imaging” IEEE press, Ch-1,pg-1-4, 1999
2. A.C. Kak and M. Slaney , “Principles of Computerised Tomographic Imaging” IEEE press, Ch-3,pg-60, 1999
3. A.C. Kak and M. Slaney , “Principles of Computerised Tomographic Imaging” IEEE press, Ch-4,pg-134,137,158, 1999
4. Max Born and Emil Wolf , “Principles of optics-Electromagnetic theory of propagation ,interference and diffraction of light”, Cambridge University press,Ch-8,pg-695-703,2005
5. J.H.Richmond, ”Scattering by a Dielectric Cylinder of Arbitrary Cross-section Shape”,IEEE transactions on Antenna and Propagation, vol. 13, No. 3, 334-341, 1965
6. A.C. Kak and M. Slaney , “Principles of Computerised Tomographic Imaging” IEEE press, Ch-6,pg-208-214,218,137,158,234-247 1999
7. G.Gbur and E.Wolf, ” Relation between Computed and Diffraction tomography”, J. Opt. Soc. Am. A/Vol. 18, No. 9/September 2001
8. C.F. Gerald and P.O. Wheatly, ”Applied Numerical Analysis”,Ch-5,pg-301,seventh edition ,Pearson.
9. Rudra Pratap, ”Getting Started with Matlab 7”,Oxford University Press
10. A.k. Kundu ,B.Bandyopadyay, ”An Image Reconstruction and Enhancement Technique for Microwave Tomography”,Abstract, ACTA TECHNICA CORVINIENSIS -Bulletin of Engineering